eprints@whiterose.ac.uk
https://eprints.whiterose.ac.uk/

letters to nature

4. Weissenhorn, W. *et al.* The ectodomain of HIV-1 env subunit gp41 forms a soluble, alpha-helical, rod-like oligomer in the absence of gp120 and the N-terminal fusion peptide. *EMBO J.* **15,** 1507–1514 (1996).

5. Modis, Y., Ogata, S., Clements, D. & Harrison, S. C. Structure of the dengue virus envelope protein after membrane fusion. *Nature* **427,** 313–319 (2004).

6. Gibbons, D. L. *et al.* Conformational change and protein-protein interactions of the fusion protein of Semliki Forest virus. *Nature* **427,** 320–325 (2004).

7. Dormitzer, P. R., Sun, Z.-Y. J., Wagner, G. & Harrison, S. C. The rhesus rotavirus VP4 sialic acid binding domain has a galectin fold with a novel carbohydrate binding site. *EMBO J.* **21,** 885–897 (2002).

8. Mackow, E. R. *et al.* The rhesus rotavirus gene encoding protein VP3: location of amino acids involved in homologous and heterologous rotavirus neutralization and identification of a putative fusion region. *Proc. Natl Acad. Sci. USA* **85,** 645–649 (1988).

9. Dowling, W., Denisova, E., LaMonica, R. & Mackow, E. R. Selective membrane permeabilization by the rotavirus VP5* protein is abrogated by mutations in an internal hydrophobic domain. *J. Virol.* **74,** 6368–6376 (2000).

10. Graham, K. L. *et al.* Integrin-using rotaviruses bind α2β1 integrin α2 I domain via VP4 DGE sequence and recognize αXβ2 and αVβ3 by using VP7 during cell entry. *J. Virol.* **77,** 9969–9978 (2003).

11. Ruggeri, F. M. & Greenberg, H. B. Antibodies to the trypsin cleavage peptide VP8 neutralize rotavirus by inhibiting binding of virions to target cells in culture. *J. Virol.* **65,** 2211–2219 (1991).

12. Offit, P. A., Shaw, R. D. & Greenberg, H. B. Passive protection against rotavirus-induced diarrhea by monoclonal antibodies to surface proteins vp3 and vp7. *J. Virol.* **58,** 700–703 (1986).

13. Dormitzer, P. R., Greenberg, H. B. & Harrison, S. C. Proteolysis of monomeric recombinant rotavirus VP4 yields an oligomeric VP5* core. *J. Virol.* **75,** 7339–7350 (2001).

14. Arias, C. F., Romero, P., Alvarez, V. & Lopez, S. Trypsin activation pathway of rotavirus infectivity. *J. Virol.* **70,** 5832–5839 (1996).

15. Gilbert, J. M. & Greenberg, H. B. Cleavage of rhesus rotavirus VP4 after arginine 247 is essential for rotavirus-like particle-induced fusion from without. *J. Virol.* **72,** 5323–5327 (1998).

16. Tihova, M., Dryden, K. A., Bellamy, A. R., Greenberg, H. B. & Yeager, M. Localization of membrane permeabilization and receptor binding sites on the VP4 hemagglutinin of rotavirus: implications for cell entry. *J. Mol. Biol.* **314,** 985–992 (2001).

17. Taniguchi, K. *et al.* Identification of cross-reactive and serotype 2-specific neutralization epitopes on VP3 of human rotavirus. *J. Virol.* **62,** 2421–2426 (1988).

18. Shaw, A. L. *et al.* Three-dimensional visualization of the rotavirus hemagglutinin structure. *Cell* **74,** 693–701 (1993).

19. Yeager, M., Berriman, J. A., Baker, T. S. & Bellamy, A. R. Three-dimensional structure of the rotavirus haemagglutinin VP4 by cryo-electron microscopy and difference map analysis. *EMBO J.* **13,** 1011–1018 (1994).

20. Liemann, S., Chandran, K., Baker, T. S., Nibert, M. L. & Harrison, S. C. Structure of the reovirus membrane-penetration protein, μ1, in a complex with its protector protein, σ3. *Cell* **108,** 283–295 (2002).

21. Weeks, C. M. & Miller, R. The design and implementation of SnB v2.0. *J. Appl. Crystallogr.* **32,** 120–124 (1999).

22. Padilla, J. E. & Yeates, T. O. A statistic for local intensity differences: robustness to anisotropy and pseudo-centering and utility for detecting twinning. *Acta Crystallogr. D* **59,** 1124–1130 (2003).

23. Crowther, R. A. Procedures for three-dimensional reconstruction of spherical viruses by Fourier synthesis from electron micrographs. *Phil. Trans. R. Soc. Lond. B* **261,** 221–230 (1971).

24. Lawton, J. A. & Prasad, B. V. V. Automated software package for icosahedral virus reconstruction. *J. Struct. Biol.* **116,** 209–215 (1996).

25. Ludtke, S. J., Baldwin, P. R. & Chiu, W. EMAN: semiautomated software for high-resolution single-particle reconstructions. *J. Struct. Biol.* **128,** 82–97 (1999).

26. Wriggers, W., Milligan, R. A. & McCammon, J. A. Situs: A package for docking crystal structures into low-resolution maps from electron microscopy. *J. Struct. Biol.* **125,** 185–195 (1999).

27. Jones, T. A., Zou, J. Y., Cowan, S. W. & Kjeldgaard, M. Improved methods for binding protein models in electron density maps and the location of errors in these models. *Acta Crystallogr. A* **47,** 110–119 (1991).

28. Kraulis, J. MOLSCRIPT: A program to produce both detailed and schematic plots of protein structures. *J. Appl. Crystallogr.* **24,** 946–950 (1991).

29. Nicholls, A., Sharp, K. A. & Honig, B. Protein folding and association: insights from interfacial and thermodynamic properties of hydrocarbons. *Prot. Struct. Funct. Genet.* **11,** 281–296 (1991).

30. Yeager, M., Dryden, K. A., Olson, N. H., Greenberg, H. B. & Baker, T. S. Three-dimensional structure of rhesus rotavirus by cryoelectron microscopy and image reconstruction. *J. Cell Biol.* **110,** 2133–2144 (1990).

....

The native architecture of a photosynthetic membrane

Svetlana Bahatyrova[1]*, **Raoul N. Frese**[1,2]*, **C. Alistair Siebert**[3],
John D. Olsen[3], **Kees O. van der Werf**[1], **Rienk van Grondelle**[2],
Robert A. Niederman[4], **Per A. Bullough**[3], **Cees Otto**[1] & **C. Neil Hunter**[3]

[1]*Biophysical Techniques Group, Department of Science & Technology, BMTI, MESA⁺, University of Twente, P.O. Box 217, 7500 AE Enschede, The Netherlands*
[2]*Biophysics, Faculty of Sciences, Vrije Universiteit Amsterdam, de Boelelaan 1081, 1081 HV, The Netherlands*
[3]*Department of Molecular Biology and Biotechnology, University of Sheffield, Sheffield S10 2TN, UK*
[4]*Rutgers University, Department of Molecular Biology and Biochemistry, Piscataway, New Jersey 08854, USA*

* These authors contributed equally to this work

....

In photosynthesis, the harvesting of solar energy and its subsequent conversion into a stable charge separation are dependent upon an interconnected macromolecular network of membrane-associated chlorophyll–protein complexes. Although the detailed structure of each complex has been determined[1–4], the size and organization of this network are unknown. Here we show the use of atomic force microscopy to directly reveal a native bacterial photosynthetic membrane. This first view of any multi-component membrane shows the relative positions and associations of the photosynthetic complexes and reveals crucial new features of the organization of the network: we found that the membrane is divided into specialized domains each with a different network organization and in which one type of complex predominates. Two types of organization were found for the peripheral light-harvesting LH2 complex. In the first, groups of 10–20 molecules of LH2 form light-capture domains that interconnect linear arrays of dimers of core reaction centre (RC)–light-harvesting 1 (RC–LH1–PufX) complexes; in the second they were found outside these arrays in larger clusters. The LH1 complex is ideally positioned to function as an energy collection hub, temporarily storing it before transfer to the RC where photochemistry occurs: the elegant economy of the photosynthetic membrane is demonstrated by the close packing of these linear arrays, which are often only separated by narrow 'energy conduits' of LH2 just two or three complexes wide.

Photosynthetic purple bacteria can contain two types of complex, RC–LH1 and LH2, with both light-harvesting complexes comprising roughly circularly arranged α-helices with bound carotenoid and bacteriochlorophyll (Bchl) pigments[3–6]. To investigate the functionally crucial organization of these complexes, native photosynthetic membranes from the wild-type purple bacterium *Rhodobacter sphaeroides* were imaged by atomic force microscopy (AFM), a technique that allows the topography of biological samples to be acquired in buffer solution at room temperature and under normal pressure. Figure 1a shows a cluster of several membrane patches, each of a size approximating to the surface area of an intracytoplasmic membrane vesicle (chromatophore). The bright areas represent photosynthetic complexes; even at this low magnification this remarkable view of native photosynthetic membranes shows that they are composed, at least in part, of linear arrays of dimeric complexes. This arrangement was mirrored in all the membrane patches we examined, and a gallery of additional images is shown in Supplementary Fig. S1.

Figure 1b clearly shows how the light-harvesting and photo-chemical functions of a membrane are apportioned, and reveals the arrangement of photosynthetic complexes. Two types can be seen: large circular complexes with a bright and therefore

protruding central protein, and smaller rings with no central density and a diameter of about 7 nm. The antenna complexes were identified by comparison with AFM data compiled on purified LH2, LH1 and RC–LH1 complexes[7–9] and the three-dimensional structures for the LH2 and LH1–RC–PufX complexes[1–4]. The larger features are RC–LH1–PufX complexes, each about 12 nm in diameter and comprising an LH1 ring surrounding a central bright region representing a RC complex. These RC–LH1–PufX complexes are usually dimeric, and the dimers are arranged in rows such as those indicated (red arrows) in Fig. 1b. Typically, rows of up to six dimers of RC–LH1–PufX complexes are found, forming a domain of 240–360 Bchl molecules. This is in close agreement with singlet–singlet annihilation experiments on a mutant containing only the RC–LH1–PufX complex that established domain sizes of 330 or more LH1 Bchl molecules at room temperature[10].

Rather than being interspersed randomly throughout the membrane, many of the LH2 complexes are clustered in regions between the rows of RC–LH1–PufX dimers, as outlined in Fig. 1c. Typically these regions consist of 10–20 LH2 complexes representing 270–540 Bchl molecules; the same order of magnitude of connected Bchl molecules (365 or more) was deduced from singlet–singlet annihilation measurements of mutant LH2-only *R. sphaeroides* membranes[10]. We suggest that the LH2 complexes situated between rows of RC–LH1–PufX dimers form a relatively invariant complement of light-harvesting antenna, and that the arrangement of complexes depicted in Fig. 1c represents the basic requirement for the efficient harvesting, transmission and trapping of light energy in this bacterium. However by itself this would not account for all the LH2 present; a comparison of the starting absorbance spectrum with one estimated from the number of LH2 and LH1 rings in Figs 1 and 2 indicates that up to 50% of the expected LH2 has not been accounted for in such images. The circled region in Fig. 2a shows that there are other regions consisting largely of LH2 that are not 'sandwiched' between rows of RC–LH1–PufX complexes. Individual LH2 rings can be discerned within the higher-magnification image in Fig. 2b, such as the one indicated with an

arrow. These LH2-enriched domains could represent the variable antenna, known for many years to form in response to a lowered light intensity[11]. In addition to making contact with each other, some of the LH2 rings are in close physical association with the RC–LH1–PufX complexes (see upper green arrow in Fig. 1b), facilitating the transfer of excitation energy from LH2 to LH1 and thence to the RC. Even at this intermediate level of detail, the physical and organizational basis for harvesting, transferring and using light energy is clearly evident.

A model of the bacterial photosynthetic membrane has been formulated in Fig. 1c (inset) by arranging the structural information available for the individual photosynthetic components[2–4] in a manner consistent with the AFM data. These direct images of an intact photosynthetic membrane resemble one of the models proposed in 1976 (ref. 12) on the basis of fluorescence-quenching experiments conducted on *R. sphaeroides* membranes. From a quantitative point of view the model in Fig. 1c explains why fluorescence-quenching studies of *R. sphaeroides* membranes concluded that there were up to 3,000 light-harvesting Bchl molecules connected for energy transfer[13]. This work also estimated that a single photosynthetic membrane vesicle would contain 30 RCs, in rough agreement with the number observed in the membrane patches in Figs 1 and 2. The AFM data suggest that 100 or more LH2 molecules would form the dominant antenna within such a vesicle, partitioned between the linear rows of RC–LH1–PufX dimers (Fig. 1c) and the LH2-enriched areas in Fig. 2b. There is extensive physical continuity between individual LH2 complexes (27 Bchl molecules for each ring) and between LH2 and RC–LH1–PufX dimers (60 LH1 Bchl molecules per dimer). Thus, the LH2 rings seem to cooperate to form an extended array for collecting photons, and, once transferred 'downhill' to a RC–LH1–PufX dimer, the excited state can hop the relatively large distance of about 3.5 nm from LH1 Bchl molecules to the special pair of Bchl molecules within the RC[14], thereby eliciting conversion to photochemical energy[15]. It is possible that the linear arrays of RC–LH1–PufX complexes cooperate in the overall process of energy trapping, because if any particular RC is already under-
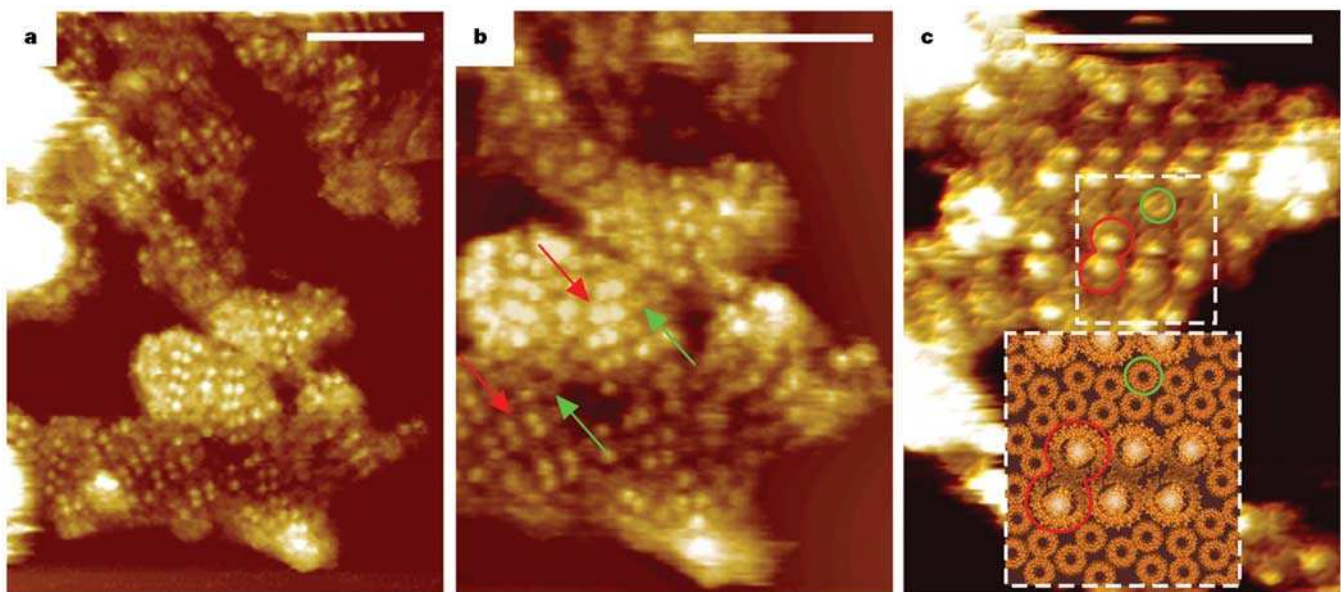
Figure 1 AFM of native photosynthetic membranes. **a**, Large-scale view of several membrane fragments. **b**, Higher-magnification view showing a region of dimeric RC–LH1–PufX core complex arrays (red arrows) and associated LH2 complexes (green arrows). **c**, Three-dimensional view of core complex arrays surrounded by LH2 complexes. The inset at the bottom is a representation of the region denoted by the dashed box in the centre, using model structures derived from atomic resolution data[2–4]. A typical RC–LH1–PufX dimer is delineated in both images by a red outline and a representative LH2 complex by a green circle. Scale bar, 100 nm in all panels. For all images the z range is 6 nm (from darkest to lightest).

taking photochemical charge separation and is thus unavailable for receiving excitation energy from its LH1 ring (in a 'closed' state), the LH1 excitation can migrate along a succession of such dimers until an 'open' RC is reached. This arrangement of RC–LH1–PufX dimers might also provide a structure with the largest number of effective connections between LH1 rings. In addition, it becomes clear why mutants lacking LH2 form tubular membranes containing linear rows of dimers aligned in parallel[9,16]; this is a natural consequence of removing the LH2 complexes that normally separate rows of RC–LH1–PufX dimers.

The AFM was used to examine a small area of membrane containing only a few photosynthetic complexes; for clarity the data are represented in three dimensions (Fig. 3). The rows of dimeric RC–LH1–PufX complexes, which are the most prominent

features in low-magnification topographs of photosynthetic membranes (Fig. 1a, b), can now be seen in greater detail. Each dimer in Fig. 3 is about 23 nm across, corresponding to the RC–LH1–PufX dimer complexes about 20 nm in width previously revealed by negative-stain electron microscopy[9]. The central protruding feature is about 4 nm above the lipid bilayer, which corresponds to the H subunit of the RC[8]. It is therefore the cytoplasmic face of the membrane that lies uppermost and the periplasmic face that has adhered to the mica substrate. Inspection of the RC–LH1–PufX dimers shows that in some cases the bright central density is missing. This has been seen before in AFM images of bacterial RCs, and it arises when the AFM tip dislodges an extrinsic subunit, revealing the underlying L and M subunits[8,17]. As seen in Fig. 1, some of the LH2 complexes make contact with RC–LH1–PufX complexes, at points indicated by the arrows in Fig. 3, fulfilling their role not only as gatherers of relatively high-energy excitations but also as energy conduits to the lower-energy LH1 complex surrounding the RC. Although LH2 complexes associate mainly with other LH2 complexes, some can be found singly, for example sandwiched between two RC–LH1–PufX complexes (Fig. 3, circle). At the contact points between LH2 and RC–LH1–PufX complexes, the distance between the B850 Bchl molecules of LH2 and the B875 Bchl molecules of LH1 was calculated to be between 2.7 and 3.2 nm on the basis of the energy transfer time constant, which is 3 ps (ref. 18). Remarkably, the subunit structure of both LH2 and LH1 light-harvesting rings emerges, even in the native membrane environment. The LH2 rings such as those marked by asterisks in Fig. 3 seem to be composed of nine units *in vivo*, which is consistent with previous structural data[3,5].
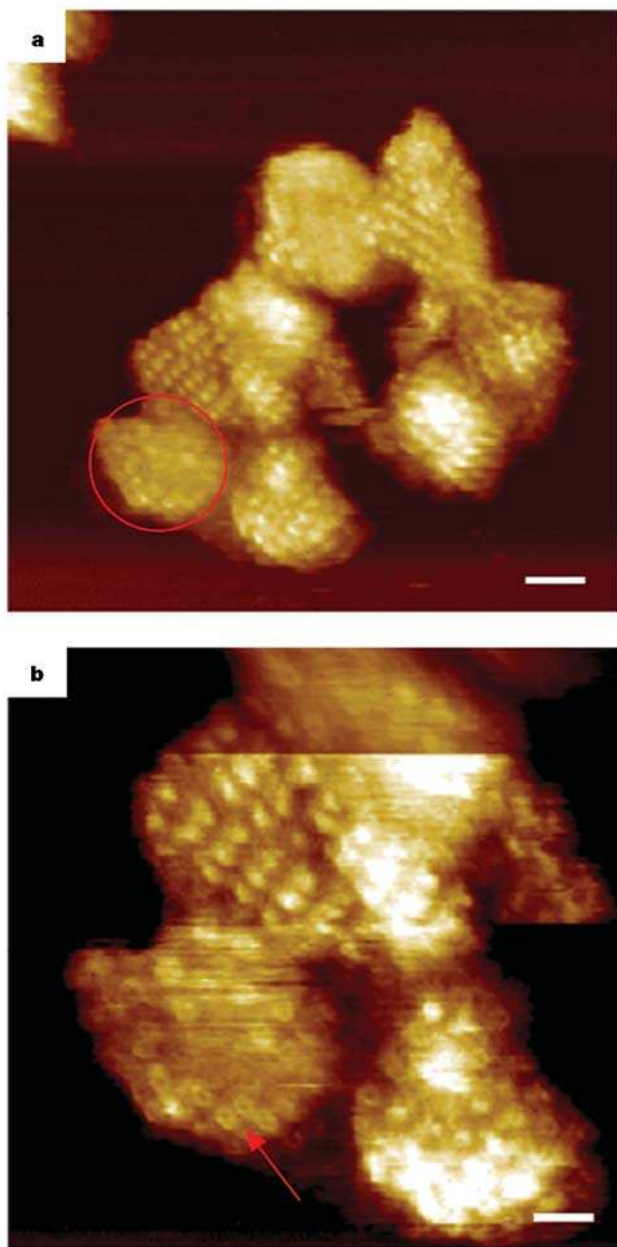

Figure 2 Membrane patches showing two types of arrangement of photosynthetic complexes. **a**, The circled region is composed mainly of LH2 complexes. **b**, Higher-magnification image of the same membrane patch in which an arrow points to an LH2 ring within the LH2-only domain. This higher-resolution scan clearly shows that there are no core complexes in these regions. Scale bar, 50 nm (**a**); 25 nm (**b**).
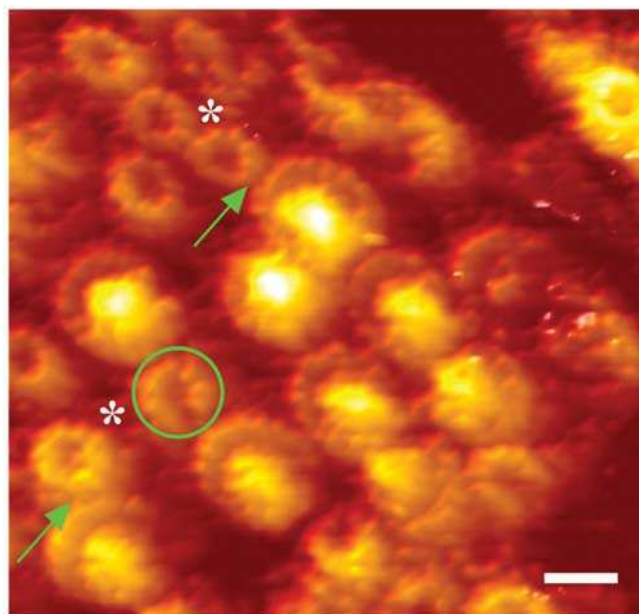

Figure 3 Three-dimensional representation of a small region of membrane showing RC–LH1–PufX core complex dimers and monomers with associated LH2 complexes. Contact points for energy transfer between LH2 and RC–LH1–PufX complexes are indicated by green arrows. LH2 rings marked by asterisks are composed of nine units. The LH2 complex in the green circle is sandwiched between two RC–LH1–PufX complexes. The average tilt of seven LH1 complexes is 4.8°; the average height of LH1 above the lipid membrane is 1.4 ± 0.3 nm (mean ± s.d.). The maximum subunit height is 1.8 ± 0.3 nm ($n = 7$) and the minimum subunit height is 1.1 ± 0.1 nm ($n = 7$). The average tilt of three LH2 complexes is 3.8°. For LH2 the average height of LH2 rings above the lipid membrane is 1.5 ± 0.2 nm ($n = 11$). For three tilted rings the maximum subunit height is 1.7 ± 0.1 nm and the minimum subunit height is 1.2 ± 0.1 nm. The average height of the reaction centre H subunit above the lipid membrane is 3.7 ± 0.3 nm ($n = 9$). Scale bar, 10 nm.

We also investigated the disposition of individual photosynthetic complexes with respect to the native membrane bilayer, information that has escaped the attention of crystallographic methods. Some, but not all, LH2 complexes seem to be slightly tilted in the native membrane, estimated to be between 3° and 4° from the vertical. This tilting is a surprise, notwithstanding the fact that LH2 is tilted in two-dimensional crystals reconstituted from detergent-purified LH2 complexes[5,19]. This phenomenon is not confined to the LH2 complex; close inspection of seven LH1 rings within a series of native RC–LH1–PufX dimers reveals an average 4.8° tilt of each LH1 ring towards the monomer–monomer interface. We cannot determine whether the enclosed RC is also tilted, although we note that purified, detergent-solubilized RCs crystallized in a cubic lipidic phase lie 11° from the vertical[20]. This small degree of tilt in each RC–LH1–PufX complex obscures the central part of each dimer from analysis, preventing the identification of the PufX polypeptide, which is thought to be somewhere in this region[9,21]. It is not clear whether the tilting of LH2 and RC–LH1–PufX complexes has any functional significance, but the mutual inward tilt of the RC–LH1–PufX complexes indicates that it might be a consequence of the dimerization process. The tilting of these photosynthetic complexes might be accompanied by a slight degree of buckling of the lipid bilayer in the immediate vicinity of the complex and could arise as a consequence of applying the sample to the mica surface, which imposes a flattened profile on a piece of membrane that was originally curved. This could be exacerbated in LH2-rich regions, which are expected to be particularly curved[22]. An interaction with the mica surface could also account for the very low lateral mobility of the photosynthetic complexes in the membrane patches that we observed. This point is illustrated by Supplementary Fig. S2, which displays four of a sequence of ten consecutive images obtained from the same membrane patch. The reproducibility of the data is remarkable, even on the scale of a single LH2 complex. A similar lack of lateral mobility was noted previously[23] in a study of the bacterial ATP synthase in a reconstituted lipid bilayer; there was remarkably low diffusion in comparison with eukaryotic membranes. In the same study, those molecules that formed close associations with others did not tend to move and some of the isolated mobile molecules ceased moving when they associated with larger groups. We suggest that the close packing of many of the light-harvesting complexes probably prevents the lateral diffusion of individual components.

This study has directly revealed the organization of bacterial photosynthetic membranes. Further questions can now be addressed: for example, how does the increased level of LH2 in low-light-grown cells affect this architecture? Where is the other component of the cyclic electron transfer chain, the cytochrome bc_1 complex, located in the cell? Where is the ATP synthase? How is this simple yet effective photosynthetic membrane assembled? Further work will be necessary to answer these questions. Only small amounts of the cytochrome bc_1 complex were detected by western blot analysis of the membrane patches (results not shown), and there could be a potential problem in detecting cytochrome bc_1 complexes by AFM, because the very recently determined structure of this complex from the photosynthetic bacterium *Rhodobacter capsulatus* reveals relatively little surface topology on the cytoplasmic side of the membrane[24]. In the case of the ATP synthase it has been reported that intracytoplasmic membrane vesicles of *R. capsulatus* contain on average only one F_oF_1-ATP synthase. Indeed, 37% of the chromatophore vesicles had no ATP synthase at all[25].

In view of the highly organized arrangements of photosynthetic complexes seen in recent electron microscopic investigations of bacterial and plant membranes[9,26], in which crystallographic order is demonstrated, our results present a slightly more chaotic landscape. A high degree of order is clearly not essential for transmitting excitation energy; the bacterial photosynthetic membrane fulfils the basic requirements of being physically extensive to maximize the likelihood of harvesting photons, while fostering multiple contacts between its light-harvesting components so that energy can migrate between complexes. In the context of its energy transfer function this is a very robust architecture, because associations between light-harvesting rings place few demands on the contact sites as long as the distances between rings are minimized. Thus, the two-dimensional organization we have revealed here by AFM will always present multiple possibilities and pathways for the fast and efficient transfer and trapping of energy. □

Methods

Bacterial growth

Cells of *R. sphaeroides* NCIB 8253 were grown photosynthetically at moderate light intensity (500 W m^{-2} for 18–20 h) and then switched to high light intensity (825 W m^{-2}) for 4 h. Intracytoplasmic membrane vesicles with an LH1/LH2 molar ratio of 0.78 were isolated by rate-zonal sucrose density gradient centrifugation[27]. Membranes were pelleted by ultracentrifugation at 100,000*g* for 4 h and resuspended with gentle homogenization in 50 mM HEPES buffer at pH 8 containing 0.03% β-dodecyl maltoside (buffer A) to 16 A_{875} units cm^{-1} ml^{-1}. A 250-µl portion of this sample was loaded on a 20/25/30/35/40/50% w/w sucrose-density step gradient in buffer A and centrifuged for 20 h at 200,000*g* with a Beckman SW41 rotor. The fraction containing large membrane fragments was harvested from the 40/50% interface with a blunted hypodermic syringe and frozen at −20 °C, with 45% sucrose as cryoprotectant, until required for AFM.

Atomic force microscopy

The sample solution was adsorbed on the surface of freshly cleaved mica (Ted Pella, Redding, California, USA). A small drop of adsorption buffer (10 mM Tris-HCl pH 7.5, 150 mM KCl, 25 mM MgCl₂) was applied to the mica surface to ensure a firm attachment of the membranes, then 1 µl of the sample was injected into the thin film of adsorption buffer and left for 1–1.5 h. The sample was then gently washed with the recording buffer (10 mM Tris-HCl pH 7.5, 150 mM KCl) and placed on the AFM stage, where 100 µl of recording buffer was added to the liquid cell. A home-built AFM was used[28]. Standard Si₃N₄ cantilevers (ThermoMicroscopes, Sunnyvale, California, USA) had a spring constant of 0.5 N m^{-1} and operating frequencies of 25–35 kHz in liquid. AFM topographs were obtained with the use of tapping mode in liquid. The images with the highest resolution were achieved when the free tapping amplitude was 1–2 nm and the amplitude setpoint was adjusted to minimal forces, resulting in the damping of the free amplitude by only 5–10%. Images contained 256 × 256 pixels and were recorded at a typical line frequency of 5–7 Hz. Quantitative analysis of the AFM topographs and three-dimensional representation of the surface structures were performed with Scanning Probe Image Processor (Image Metrology ApS, Lyngby, Denmark).

1. Deisenhofer, J., Epp, O., Miki, K., Huber, R. & Michel, H. Structure of the protein subunits in the photosynthetic reaction centre of *Rhodopseudomonas viridis* at 3 Å resolution. *Nature* **318,** 618–624 (1985).
2. Allen, J. P., Feher, G., Yeates, T. O., Komiya, H. & Rees, D. C. Structure of the reaction center from *Rhodobacter sphaeroides* R26: The protein subunits. *Proc. Natl Acad. Sci. USA* **84,** 6162–6166 (1987).
3. McDermott, G. *et al.* Crystal structure of an integral membrane light-harvesting complex from photosynthetic bacteria. *Nature* **374,** 517–521 (1995).
4. Roszak, A. W. *et al.* Crystal structure of the RC-LH1 core complex from *Rhodopseudomonas palustris*. *Science* **302,** 1969–1972 (2003).
5. Walz, T., Jamieson, S. J., Bowers, C. M., Bullough, P. A. & Hunter, C. N. Projection structures of three photosynthetic complexes from *Rhodobacter sphaeroides*: LH2 at 6 Å, LH1 and RC-LH1 at 25 Å. *J. Mol. Biol.* **282,** 833–845 (1998).
6. Jamieson, S. J. *et al.* Projection structure of the photosynthetic reaction centre-antenna complex of *Rhodospirillum rubrum* at 8.5 Å resolution. *EMBO J.* **21,** 3927–3935 (2002).
7. Bahatyrova, S. *et al.* Flexibility and size heterogeneity of the LH1 light harvesting complex revealed by atomic force microscopy: functional significance for bacterial photosynthesis. *J. Biol. Chem.* **279,** 21327–21333 (2004).
8. Fotiadis, D. *et al.* Structural analysis of the RC-LH1 photosynthetic core complex of *Rhodospirillum rubrum* using atomic force microscopy. *J. Biol. Chem.* **279,** 2063–2068 (2004).
9. Siebert, C. A. *et al.* Molecular architecture of photosynthetic membranes in *Rhodobacter sphaeroides*: the role of PufX. *EMBO J.* **23,** 690–700 (2004).
10. Vos, M. H., van Dorssen, R. J., Amesz, J., van Grondelle, R. & Hunter, C. N. The organisation of the photosynthetic apparatus of *Rhodobacter sphaeroides*: studies of antenna mutants using singlet-singlet quenching. *Biochim. Biophys. Acta* **933,** 132–140 (1988).
11. Aagaard, J. & Siström, W. R. Control of synthesis of reaction centre bacteriochlorophyll in photosynthetic bacteria. *Photochem. Photobiol.* **15,** 209–225 (1972).
12. Monger, T. & Parson, W. W. Singlet-triplet fusion in *Rhodopseudomonas sphaeroides*. *Biochim. Biophys. Acta* **460,** 393–407 (1977).
13. Hunter, C. N., Kramer, H. J. M. & van Grondelle, R. Linear dichroism and fluorescence emission of antenna complexes during photosynthetic unit assembly in *Rhodopseudomonas sphaeroides*. *Biochim. Biophys. Acta* **807,** 44–51 (1985).
14. Visscher, K. J., Bergström, H., Sundström, V., Hunter, C. N. & van Grondelle, R. Temperature-dependence of energy-transfer from the long wavelength antenna BChl-896 to the reaction centre in *Rhodospirillum rubrum*, *Rhodobacter sphaeroides* (w.t. and M21 mutant) from 77 to 177K, studied by

letters to nature

picosecond absorption spectroscopy. *Photosyn. Res.* **22,** 211–217 (1989).

15. Beekman, L. M. *et al.* Trapping kinetics in mutants of the photosynthetic purple bacterium *Rhodobacter sphaeroides*: influence of the charge separation rate and consequences for the rate-limiting step in the light-harvesting process. *Biochemistry* **33,** 3143–3147 (1994).

16. Frese, R. N. *et al.* The long-range supraorganization of the bacterial photosynthetic unit: A key role for PufX. *Proc. Natl Acad. Sci. USA* **97,** 5197–5202 (2000).

17. Scheuring, S. *et al.* Nanodissection and high-resolution imaging of the *Rhodopseudomonas viridis* photosynthetic core complex in native membranes by AFM. *Proc. Natl Acad. Sci. USA* **100,** 1690–1693 (2003).

18. Hess, S. *et al.* Temporally and spectrally resolved subpicosecond energy transfer within the peripheral antenna complex (LH2) and from LH2 to the core antenna complex in photosynthetic purple bacteria. *Proc. Natl Acad. Sci. USA* **92,** 12333–12337 (1995).

19. Scheuring, S. *et al.* AFM characterization of tilt and intrinsic flexibility of *Rhodobacter sphaeroides* light harvesting complex 2 (LH2). *J. Mol. Biol.* **325,** 569–580 (2003).

20. Katona, G., Andreasson, U., Landau, E. M., Andreasson, L. E. & Neutze, R. Lipidic cubic phase crystal structure of the photosynthetic reaction centre from *Rhodobacter sphaeroides* at 2.35 angstrom resolution. *J. Mol. Biol.* **331,** 681–692 (2003).

21. Scheuring, S. *et al.* Structural role of PufX in the dimerization of the photosynthetic core-complex of *Rhodobacter sphaeroides*. *J. Biol. Chem.* **279,** 3620–3626 (2004).

22. Sturgis, J. N. & Niederman, R. A. The effect of different levels of the B800–850 light-harvesting complex on intracytoplasmic membrane development in *Rhodobacter sphaeroides*. *Arch. Microbiol.* **165,** 235–242 (1996).

23. Müller, D. J. *et al.* Observing membrane protein diffusion at subnanometer resolution. *J. Mol. Biol.* **327,** 925–930 (2003).

24. Berry, E. A. *et al.* X-ray structure of *Rhodobacter capsulatus* cytochrome bc_1: Comparison with its mitochondrial and chloroplast counterparts. *Photosyn. Res.* (in the press).

25. Feniouk, B. A., Cherepanov, D. A., Voskoboynikova, N. E., Mulkidjanian, A. Y. & Junge, W. Chromatophore vesicles of *Rhodobacter capsulatus* contain on average one F_oF_1-ATP synthase each. *Biophys. J.* **82,** 1115–1122 (2002).

26. Boekema, E. J., van Breemen, J. F., van Roon, H. & Dekker, J. P. Arrangement of photosystem II supercomplexes in crystalline macrodomains within the thylakoid membrane of green plant chloroplasts. *J. Mol. Biol.* **301,** 1123–1133 (2000).

27. Niederman, R. A., Mallon, D. E. & Parks, L. C. Membranes of *Rhodopseudomonas sphaeroides*. VI. Isolation of a fraction enriched in newly synthesized bacteriochlorophyll α-protein complexes. *Biochim. Biophys. Acta* **555,** 210–220 (1979).

28. Van der Werf, K. O. *et al.* Compact stand-alone atomic force microscope. *Rev. Sci. Instrum.* **64,** 2892–2897 (1993).

....

corrigendum

Germline stem cells and follicular renewal in the postnatal mammalian ovary

Joshua Johnson, Jacqueline Canning, Tomoko Kaneko, James K. Pru & Jonathan L. Tilly

Nature **428,** 145–150 (2004).

In this Article, we estimated that germline stem cells generate approximately 77 new primordial oocytes per day in ovaries of postnatal female mice. It has since been drawn to our attention by Ton Schumacher that a line of reasoning used in our study to verify this value is circular. However, the initial value for daily oocyte renewal obtained from mathematical modelling is not derived from a circular argument. Accordingly, this oversight does not alter any of the data or the conclusions in our paper. □